Energy Proceedings
Vol 57, 2025
ISSN 2004-2965

Research on phase behavior, flow assurance, and energy efficiency optimization in the reinjection transport process of impurity-containing CO_2

Jiao Zhou [1], Xuewen Cao [2*], Xingwang Zhang [3]
1 College of Pipeline and Civil Engineering, China University of Petroleum (East China), Qingdao 266580, China;
2 CNOOC EnerTech Equipment Technology Co., Ltd., Tianjin 300450, China
(*Corresponding Author: caoxw@upc.edu.cn)

ABSTRACT

The reinjection technology of impurity-containing CO_2 represents a critical challenge to the safety and economic viability of carbon capture and storage (CCS) systems. This study systematically analyzes the influence patterns of impurities on CO_2 phase behavior, flow characteristics, and reinjection energy consumption through the establishment of thermodynamic phase equilibrium models, flow assurance models, and energy consumption optimization models. By utilizing the Peng-Robinson (PR) equation of state and Aspen HYSYS software, the differential regulatory mechanisms of various impurities (e.g., N_2, H_2) on CO_2 critical point shifts, phase envelope expansion, and property parameters (density, viscosity, thermal conductivity) was revealed. Through OLGA multiphase flow simulations, we quantified the low-temperature risks induced by the Joule-Thomson effect and hydrate formation potential, demonstrating that impurity-containing CO_2 exhibits 2.66°C less throttling temperature drop compared to pure CO_2, with the critical hydrate formation temperature decreasing from 10°C to 8°C. For the Snohvit field case in Norway, a reinjection scheme integrating four-stage compression with interstage air cooling optimization was proposed. This high-temperature reinjection strategy (50°C) achieved 24.8% lower total energy consumption than conventional low-temperature injection (20°C), while recommending further efficiency improvements through waste heat recovery and intelligent control. The findings provide theoretical foundations and technical pathways for the safe transportation and efficient reinjection of impurity-containing CO_2.

Keywords: Impurity-containing CO_2; Phase behavior; Flow assurance; Energy efficiency optimization; Carbon capture and storage (CCS)

INTRODUCTION

Driven by global carbon neutrality targets, carbon capture, utilization and storage (CCUS) technology is recognized as a core pathway to achieve deep industrial decarbonization[1-3]. However, industrially captured CO_2 often contains impurity components such as N_2, H_2, H_2S, Ar, etc., whose altered thermodynamic and transport properties significantly affect pipeline transportation safety and storage efficiency[4-6]. Existing studies focus on the phase behavior and flow characteristics of pure CO_2[7,8], while key bottlenecks remain in the critical point shift mechanism, multiphase flow risk, and energy optimization for the impurity-containing CO_2 system.

Previous studies mainly focused on the following three aspects: (1) phase equilibrium prediction: although the GERG-2008 equation[9] and the PR equation of state[10] are widely used in the calculation of the physical properties of pure CO_2, they lack the universality of the critical point shift law for the multi-impurity mixed system[11,12]. For instance, the critical temperature drop reaches up to 30% for N_2 contents above 20%[6], while H_2 significantly expands the phase envelope [13], but the multi-impurity synergistic effect has not been quantified[14]. (2) Flow risk: Low-temperature embrittlement and hydrate generation induced by the Joule-Thomson effect are the main challenges in tubing transportation[13,15]. The temperature drop of pure CO_2 venting can reach 107.6°C[16], but the H_2-containing system will reduce the temperature drop due to the negative Joule-Thomson (J-T) coefficient[14]. In addition, transient simulations under dynamic conditions (e.g., OLGA software) mostly ignore the dynamic effects of impurities on the hydrate generation boundary[15,17]. (3) Energy consumption optimization: Snohvit and Sleipner engineering cases show that multi-stage pressurization with interstage cooling is a necessary

This is a paper for International CCUS Conference 2025 (ICCUSC 2025), May 28-29, 2025, Beijing, China.

solution[18,19], but existing models underestimate the energy consumption of interstage cooling by about 20% to 30%[20], and there is a lack of empirical evidence for the synergistic optimization of intelligent control and waste heat recovery[21,22]. Overall, the existing studies have not yet developed a systematic framework for the multi-scale coupling mechanism of impurity-phase-flow-energy consumption[23-25].

In this paper, we address the above deficiencies and systematically study the key scientific and engineering issues in impurity-containing CO_2 reinjection by integrating thermodynamic modeling, transient multiphase flow simulation and energy consumption optimization methods. The main contents include (1) constructing a phase equilibrium model of impurity-containing CO_2 based on PR equations to quantify the effects of impurities on phase envelopes, critical points, and physical properties; (2) quantifying the effects of impurities on the Joule-Thomson effect and hydrate generation, and revealing the key boundary conditions for flow assurance; and (3) proposing a synergistic optimization scheme of four-stage pressure boosting and intelligent control to validate the potentials of energy-efficiency enhancement by using real engineering examples. The study aims to provide theoretical basis and technical reference for the design, risk prevention and control, and energy efficiency improvement of impurity-containing CO_2 pipeline transmission system.

1. MODELS AND METHODS

1.1 Thermodynamic phase equilibrium model of CO_2 with impurities

In the CO_2 pipeline transportation process, the fluid temperature and pressure in the pipeline change due to many external factors (e.g., inlet conditions, elevation, and surrounding environment), which causes the fluid to produce phase changes[26]. The phase state of the fluid determines the operating condition of the pipeline, which is crucial for the transportation efficiency, safety and economy of pipeline transportation. Therefore, a full understanding of the phase characteristics of impurity-containing CO_2 helps to provide a theoretical basis for the transportation system[27].

For CO_2 pipeline, the safe and stable flow of CO_2 pipeline should be guaranteed firstly, and CO_2 pipeline is different from natural gas pipeline, which is necessary to ensure that no two-phase flow is formed in the pipeline, and also to ensure the stability of physical parameters in the flow process[28,29], among which the density change rule in the pipeline is more important for the safety of pipeline transportation. Therefore, the density-preferred equation of state is more suitable for the physical property calculation of CO_2 piping process[30].

Considering the subsequent need to carry out numerical simulation for the physical properties of multi-component impurity-containing CO_2 and the pressurization characteristics of pipeline transport, there are four main equations of state used for the calculation of substances in the commonly used engineering simulation software HYSYS, for example, namely, SRK equation, PR equation, PRSV equation, and BWRS equation[31]. In order to ensure the accuracy of the model created in the simulation software, the calculation accuracy of different equations of state in HYSYS software is compared. In the calculation of mixtures containing CO_2, the GERG-2008 equation was found to have a fairly high accuracy, but since the physical properties packages for these two equations of state were not available in the calculation software, the subsequent calculations only compared the calculation accuracy of the other four equations.

Currently, the thermal property calculation software REFPROP developed by the National Institute of Standards and Technology (NIST) is considered to be the most accurate thermal property calculation software[32,33]. The calculation results of the four types of equations of state were compared with those of REFPROP to analyze the errors for the preferences.

The four equations mentioned above were used to calculate the density values of impurity-containing CO_2 from 30 to 110°C at pressures of 7 MPa, 10 MPa and 13 MPa, respectively, and the calculated values were compared and analyzed with the calculated results of REFPROP, as shown in Fig. 1.

Table 1 Mean error between experimental and calculated values

Equation of state	PR	SRK	BWRS	PRSV
Average error/%	1.89	3.57	2.41	2.45

By comparing the prediction accuracies of the PR, SRK, BWRS, and PRSV equations of state for the physical property parameters of the impurity-containing CO_2 system (Table 1), the PR equation showed optimal engineering applicability. The average error between the calculated values of the PR equation and the experimental data was only 1.89%, which was significantly lower than that of SRK (3.57%), BWRS (2.41%), and PRSV (2.45%), indicating that the PR equation was able to more accurately capture the critical point shift characteristics and the gas-liquid equilibrium behaviors of the impurity-containing CO_2. Therefore, the PR equation is adopted as the core model for the phase equilibrium calculation and physical property parameters of the impurity-containing CO_2 system, which provides a reliable theoretical support for the process design and safety assessment of carbon capture and storage (CCS) systems.

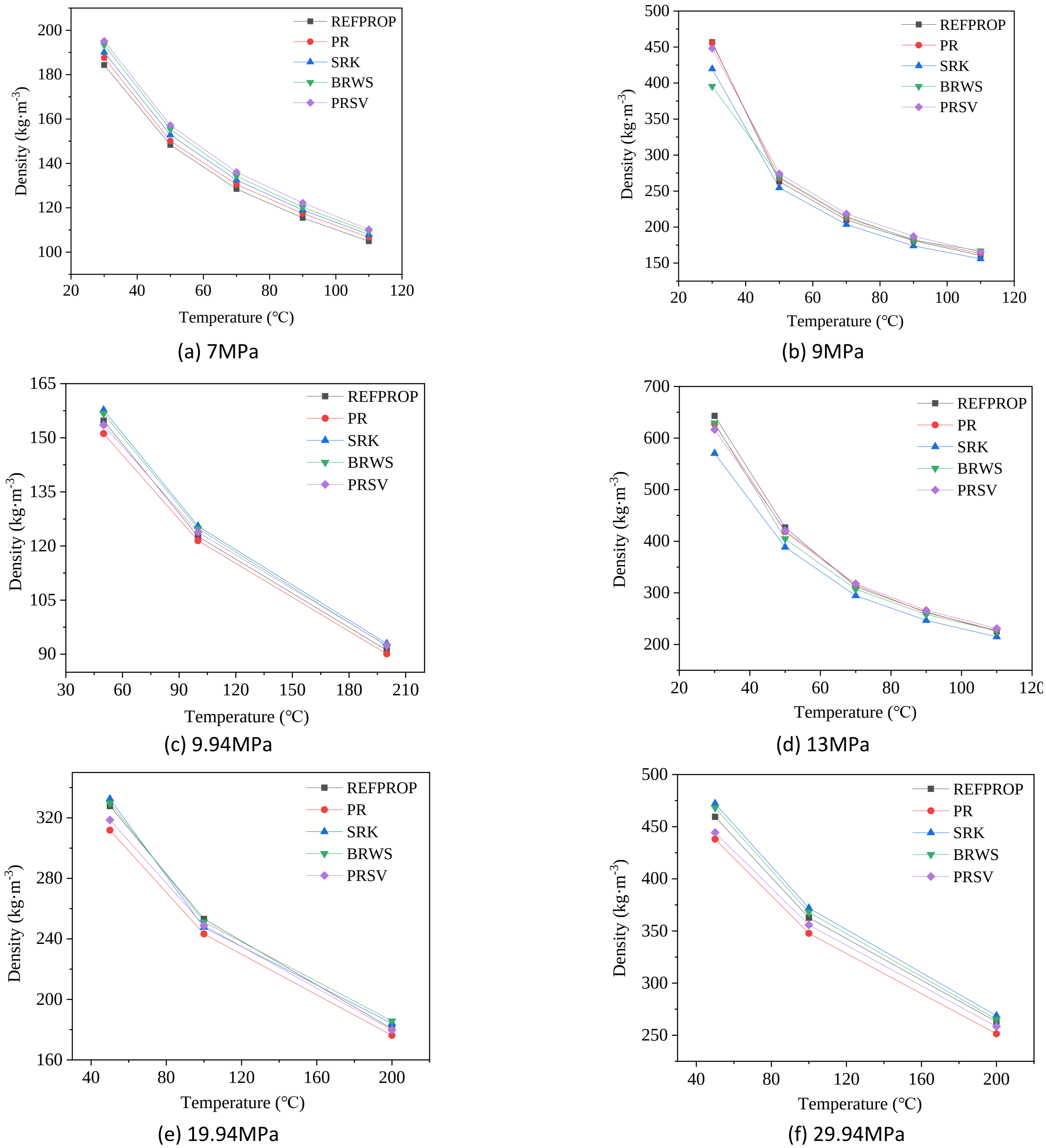

Fig. 1 Comparison of calculated values of density of CO2 containing impurities

1.2 Impurity-containing CO_2 flow safeguard modeling

In the process of CO_2 pipeline transportation and reinjection, the Joule-Thomson effect (JT effect) induced by throttling down the pressure can lead to a significant temperature drop phenomenon, which poses a potential threat to the low-temperature embrittlement of the pipe and the flow assurance[13,34]. To quantify the temperature drop characteristics of the impurity-containing CO_2 system, the thermodynamic model of the throttling process for pure CO_2 and impurity-containing

CO_2 (components as shown in Table 2) was constructed in this study using the PR equation of state based on Aspen HYSYS software. Under identical initial conditions (pressure, temperature), the temperature evolution under the condition of venting to atmospheric pressure (0.1 MPa) was simulated.

To further evaluate the flow risk in low temperature environment, the model of impurity-containing CO_2 pipeline transmission system was constructed by using OLGA transient multiphase flow simulation software. The influence of temperature-pressure distribution along the pipeline on the hydrate generation potential was analyzed by coupling thermodynamic parameters.

Table 2 Impurity-containing CO_2 components

Components	mol/%
Ar	0.6109
N_2	51.2168
CO	0.1193
CO_2	45.1104
H_2S	0.0133
H_2O	0.0114
H_2	2.9144
COS	0.0035

1.3 Energy consumption optimization model for reinjection of CO_2 containing impurities

Based on the operation goal of energy saving and emission reduction, some land terminals treat and pressurize the impurity-containing CO2 gas and then transport it through submarine pipelines for reinjection, and this model is adopted in the case of Snohvit in Norway. The method of gas treatment and pressurization at land terminals can reduce the investment cost of offshore platform construction. Most of the pressurization adopts four-stage pressurization and inter-stage cooling. Cooling can be done by air-cooling, with CO2 re-injected through a subsea module. This model is used as an example to optimize the energy consumption of CO2 reinjection with impurities.

The modeled formation conditions refer to the Norwegian Sleipner case [35,36]. It is assumed that the formation pressure is 10MPa, and the total length of the riser is 800m, including 300m of submerged riser and 500m of riser in the sandstone layer, and the main material of the riser is carbon steel, with casing and water-insulating casing wrapped around the outer layer. The seawater temperature is 3.5 ℃, the stratum temperature considering the temperature gradient, and 0.03℃/m. The stratum temperature is 35℃. The land horizontal conveying is done by uninsulated conveying, the pipe conveying material is carbon steel, the total length of the pipeline is 5km, and the ambient temperature is 20℃.

HYSYS software was used to model the reinjection pressurization before conveying, as shown in Figure 2. The model adopts four-stage pressurization, and air cooling is used between stages.

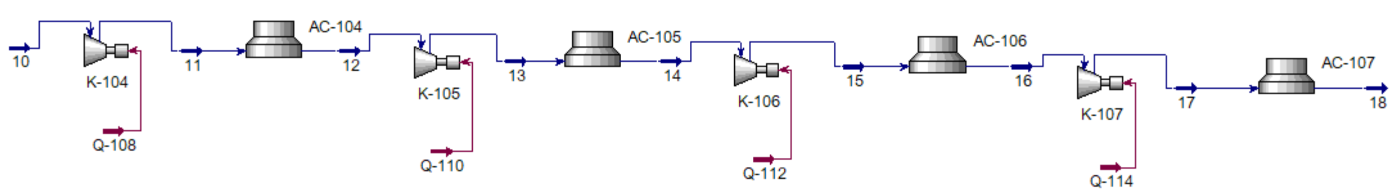

Fig. 2 Aspen HYSYS model of CO_2 pressurization with impurities

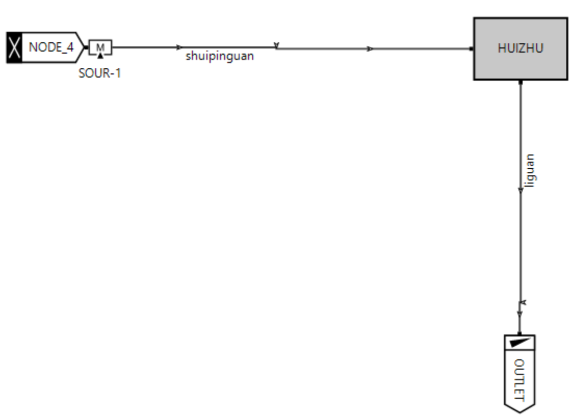

Fig. 3 OLGA modeling of impurity-containing CO_2 reinjection

Considering the reinjection from the aspects of safety and economy, there will be two cases of high-temperature reinjection and low-temperature reinjection for impurity-containing CO2. High-temperature reinjection assumes that the temperature of the outlet after cooling of the four-stage pressurization (the 18th logistics temperature in Fig. 2) is 50℃, while the low-temperature reinjection is 20℃. According to the temperature at this point, combined with the stratigraphic conditions of the reinjection, the OLGA software can be used to calculate inversely the pressure at this point. The OLGA model used is shown in Fig. 3.

2. RESULTS AND DISCUSSION

2.1 Effects of impurities on CO_2 phase equilibrium and physical properties

(1) Effect of impurities on CO_2 phase equilibrium

Given the substantial concentration of nitrogen (N_2) as a predominant impurity in CO_2-containing mixtures, N_2 serves as the principal determinant influencing the physicochemical properties of CO_2. Excluding hydrogen (H_2) and N_2, the cumulative content of remaining impurities constitutes less than 1 mol%. To methodically investigate the effects of impurity composition and concentration variations on the physical property parameters of CO_2 within impurity-laden systems, the molar fractions of impurity components were configured as follows:

1) 1% impurities + 99% CO_2;
2) 3% H_2 + 97% CO_2;
3) 50% N_2 + 50% CO_2.

Fig. 4 shows the effect on the phase diagram of CO2 when the content of all impurities is 1%. Figure 5 shows the effect on the phase diagram of CO2 when the content of impurities other than H2 is 1%.

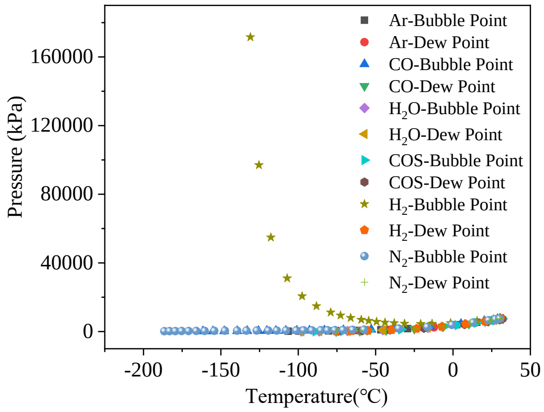

Fig. 4 Effect of each 1% impurity on the phase diagram of CO_2

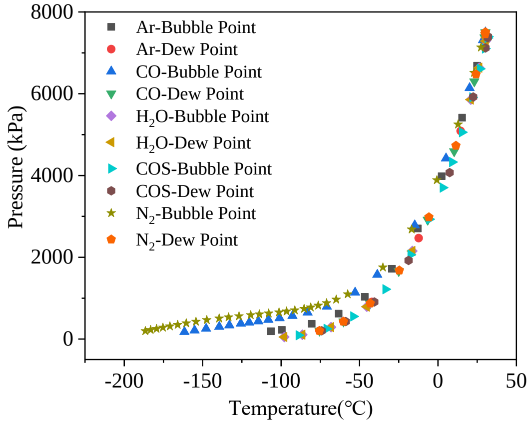

Fig. 5 Effect of each 1% impurity except H_2 on CO_2 phase diagrams

As demonstrated in Fig. 4 and Fig. 5, impurity components expand the two-phase region of the phase envelope. A 1% H_2 concentration induces substantial modifications to the bubble point curve of the CO_2 phase diagram, while exerting negligible influence on the dew point curve. With the exception of H_2O, nearly all impurities at 1% concentration alter the CO_2 phase diagram, though H_2O exhibits no measurable impact. The relative magnitude of influence follows the hierarchy: H_2 > N_2 > CO > Ar > COS > H_2S > H_2O. The presence of most impurity components predominantly alters the system's bubble point curve, while leaving the dew point curve largely unaffected.

Given the elevated concentrations of H_2 and N_2 in impurity-containing CO_2 systems, their individual concentration-dependent effects on CO_2 phase behavior warrant separate investigation. The resultant phase characteristic variations are quantified in Fig. 6 and Fig. 7.

The phase envelope area expands with increasing impurity concentrations. The addition of 3% H_2 induces further expansion of the bubble point curve while exerting minimal impact on the dew point curve and causing negligible alterations to the CO_2 critical point. In contrast, 50% N_2 substantially modifies the CO_2 critical point due to its elevated concentration, critically influencing the phase diagram, phase distribution, and critical parameter variations of the mixed system. Specifically, the presence of 50% N_2 elevates the critical pressure by a factor of 2.64 and reduces the critical temperature by 66.21°C, necessitating gaseous phase transportation for such systems.

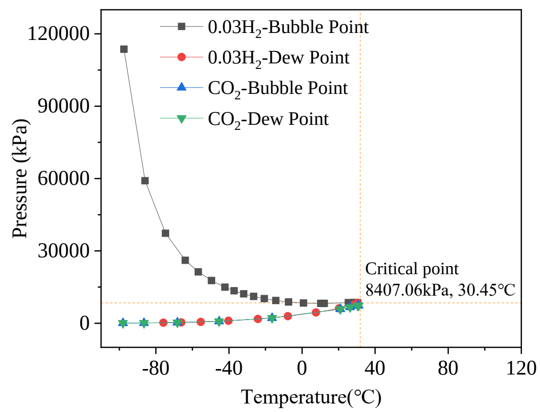

Fig. 6 Effect of 3% H_2 on the phase diagram of CO_2

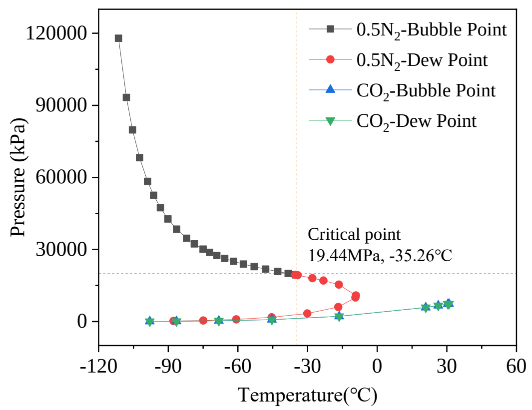

Fig. 7 Effect of 50% N_2 on the phase diagram of CO_2

As evidenced by these findings, the critical point magnitude governs the fluid transportation phase within pipelines. Consequently, a systematic evaluation of impurity-specific impacts on CO_2 critical points was conducted, with quantitative results summarized in Table 3.

Table 3 Effects of various impurities on the CO_2 critical point

Impurity type	Critical Pressure (MPa)	Comparison with pure CO_2 critical pressure (MPa)	Critical temperature (℃)	Comparison with pure CO_2 critical temperature (℃)
1%H_2	7.705	0.335	30.785	-0.165
1%N_2	7.504	0.134	30.275	-0.675
1%CO	7.502	0.132	30.262	-0.688
1%Ar	7.466	0.096	30.336	-0.614
1%COS	7.398	0.028	31.91	0.96
3%H_2S	7.388	0.018	31.52	0.57
1%H_2O	7.37	0	30.95	0
Pure CO_2	7.37	-	30.95	-

As evidenced in Table 3, impurities at equivalent concentrations exhibit differential impacts on the critical pressure and temperature of CO_2, with the hierarchy of influence being H_2 > N_2 > CO > Ar > COS > H_2S > H_2O. All impurities elevate the system's critical pressure, while only COS and H_2S increase the critical temperature; other impurities reduce it. Notably, H_2O exerts no measurable influence on the CO_2 critical point. Given the elevated N_2 concentration in the studied mixed systems, its impact dominates the overall impurity effects on CO_2.

(2) Impurity Effects on CO_2 Physical Properties

The introduction of substantial non-condensable gases (e.g., H_2, N_2, CO) in impurity-containing CO_2 systems significantly alters its physical properties—including density, viscosity, and specific heat—compared to pure CO_2. In industrially captured CO_2 streams, the presence of these non-condensable components induces marked deviations in thermodynamic properties, directly affecting phase stability, heat/mass transfer efficiency, and posing operational risks such as multiphase flow, hydrate formation, and pressure fluctuations. To address this, a multicomponent CO_2 thermodynamic model was developed using the Peng-Robinson (PR) equation of state within the Aspen HYSYS process simulation platform, enabling quantitative analysis of impurity-induced property variations. The thermophysical properties of impurity-laden CO_2 under varying temperatures and pressures are illustrated in Fig. 8.

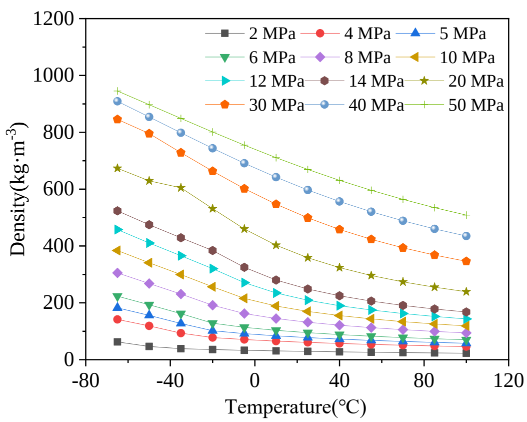

(a) Density

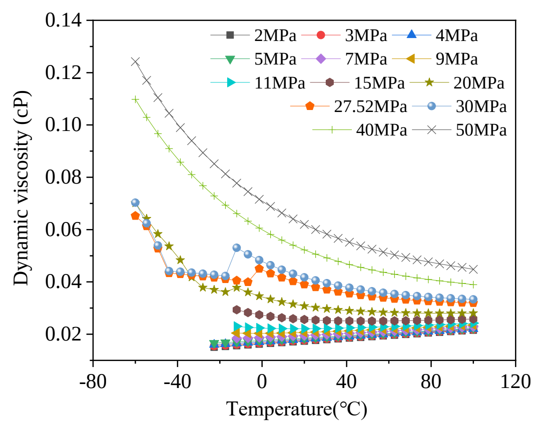

(b) Viscosity

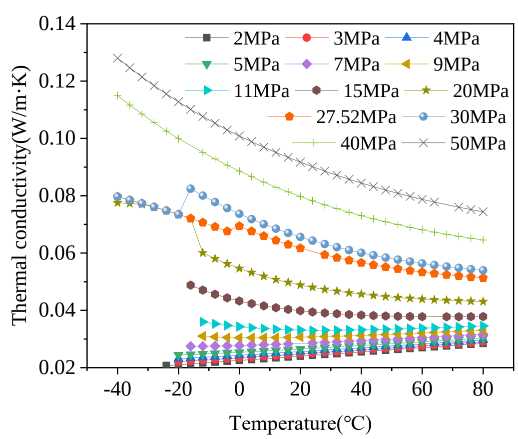

(c) Thermal conductivity

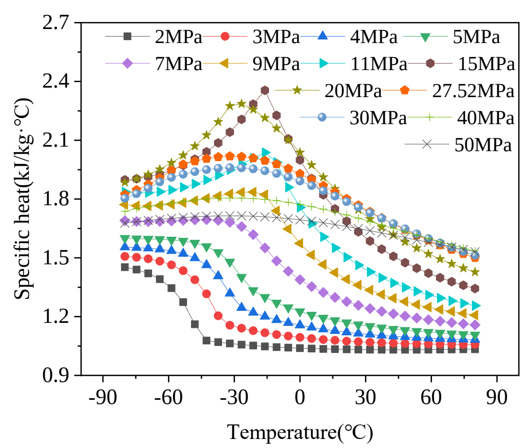

(d) Specific heat

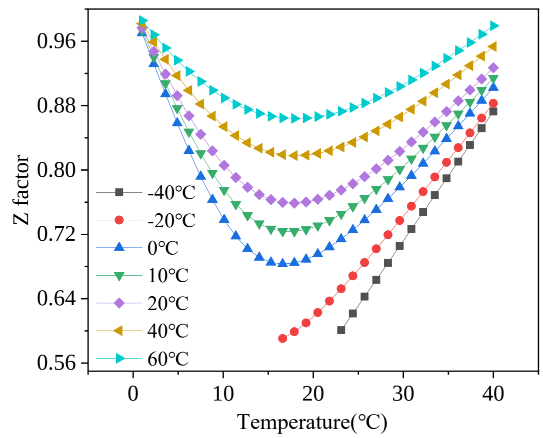

(e) Z-factor

Fig. 8 Changing law of physical properties of impurity-containing CO_2

The density variation characteristics of impurity-containing CO_2 are illustrated in Figure 9(a). The figure demonstrates significant discrepancies between the density of impurity-containing CO_2 and that of pure CO_2. Compared to pure CO_2, a general decrease in density was observed for impurity-containing CO_2, with the reduction magnitude intensifying under higher pressures. At constant pressure, density progressively diminishes with increasing temperature. Conversely, at constant temperature, density increases with rising pressure. No abrupt density transitions are observed near the critical pressure, indicating stable variations throughout the tested range.

The viscosity behavior of impurity-containing CO_2 is shown in Figure 9(b). The viscosity of impurity-containing CO_2 is lower than that of pure CO_2 due to the predominance of non-condensable components in the impurities, which maintain the system in the gaseous phase under most pressure-temperature conditions. Gas-phase viscosity is inherently lower than that of the liquid phase. At constant temperature, viscosity increases with pressure. For pressures below 15 MPa, viscosity rises with temperature. Conversely, at pressures exceeding 15 MPa, viscosity decreases with temperature. Near the critical pressure, viscosity fluctuations occur at −10°C. Under low-pressure conditions (<5 MPa) and temperatures above 0°C, the viscosity of impurity-containing CO_2 remains at minimal values.

As shown in Fig.9(c), the thermal conductivity of impurity-containing CO_2 is reduced compared to pure CO_2. Since the impurity-containing CO_2 predominantly exists in the gaseous phase under most conditions, no abrupt changes in thermal conductivity caused by phase transitions are observed. At constant temperature, thermal conductivity gradually increases with rising pressure. For pressures below 10 MPa, thermal conductivity increases with temperature. Conversely, at pressures exceeding 10 MPa, thermal conductivity decreases with temperature. Near the critical pressure, thermal conductivity exhibits fluctuations at 20℃. Under low-pressure conditions (<5 MPa) and temperatures above 0°C, the thermal conductivity of impurity-containing CO_2 remains at minimal values.

Fig. 9(d) demonstrates that at pressures greater than 20 MPa, the specific heat of impurity-containing CO_2 slightly decreases relative to pure CO_2, with the reduction magnitude intensifying at elevated temperatures. Between 15 MPa and 20 MPa, the specific heat of impurity-containing CO_2 marginally exceeds that of pure CO_2. However, within the 10–15 MPa range, it becomes slightly lower. Below 10 MPa, the specific heat values of both systems are comparable, though impurity-containing CO_2 exhibits no abrupt changes near the critical point and instead shows a gradual declining trend with increasing temperature. A minor discontinuity in specific heat occurs near 15 MPa for impurity-containing CO_2. At pressures below 5 MPa and temperatures above 0°C, the specific heat of impurity-containing CO_2 remains at low magnitudes.

As illustrated in Fig. 9(e), the Z-factor of impurity-containing CO_2 differs markedly from that of pure CO_2 under identical conditions. This discrepancy arises primarily because pure CO_2 undergoes phase transitions within narrow temperature-pressure ranges, resulting in significant Z-factor variations between phases. For impurity-containing CO_2, the critical pressure and temperature are 27.52 MPa and −52.83°C, respectively, necessitating gaseous phase transportation in practical pipeline systems. When temperatures are below 0°C, the Z-factor increases with pressure. At temperatures above 0°C, the Z-factor initially decreases and then increases, with a minimum value occurring near 16 MPa. At constant pressure, the Z-factor of impurity-containing CO_2 rises with increasing temperature.

2.2 Flow Assurance Analysis for Impurity-Containing CO_2

A thermodynamic model for the throttling processes of both pure CO_2 and impurity-containing CO_2 was developed using the PR equation of state within the Aspen HYSYS software platform. The thermodynamic simulation results under identical initial conditions are presented in Table 4.

Table 4 Low-Temperature Simulation Results

Components	Initial pressure (MPa)	Initial temperature (℃)	End Pressure (MPa)	End temperature (℃)	Temperature difference (℃)

	4.0	33.8	0.1	-14.85	48.65
Pure CO_2	7.9	33.4	0.1	-87.63	121.03
	9.2	17.4	0.1	-87.63	105.03
	15	20	0.1	-87.63	107.63
	4.0	33.8	0.1	11.7	43.154
Impurity CO_2	7.9	33.4	0.1	-11.01	49.8
	9.2	17.4	0.1	-41.78	67.21
	15	20	0.1	-71.12	104.97

As evidenced in Table 4, the throttling temperature drops of pure CO_2 and impurity-containing CO_2 systems exhibit significant differences, revealing the regulatory mechanisms of impurities on the Joule-Thomson (J-T) effect. Under identical initial conditions (15 MPa, 20°C), pure CO_2 experiences a temperature drop of 107.63°C when depressurized to atmospheric pressure, whereas the impurity-containing system shows a reduced drop of 104.97°C—a 2.66°C attenuation. These results demonstrate that light impurities attenuate overall cooling via negative J-T coefficients. Further analysis indicates that pure CO_2 exceeds its critical pressure (7.38 MPa) at an initial pressure of 7.9 MPa. Its supercritical fluid properties induce drastic expansion cooling (final temperature: –87.63°C), with the final temperature remaining constant despite decreasing initial temperatures from 33.4°C to 17.4°C, reflecting the temperature plateau effect in the supercritical region.

In contrast, impurity-containing systems exhibit elevated critical pressures (e.g., 9.8 MPa for the tested mixture). At 9.2 MPa, they remain in the gaseous phase, achieving a final temperature of only –41.78°C—significantly higher than pure CO_2 (–87.63°C). This phenomenon demonstrates that impurities reduce J-T cooling sensitivity in high-pressure segments by altering critical properties and phase distributions. Nevertheless, low-temperature risks remain non-negligible (final temperatures consistently below –40°C).

To further assess flow risks under cryogenic conditions, OLGA software was employed to analyze impurity effects on CO_2 hydrate formation potential, as detailed in Fig. 9 and Fig. 10.

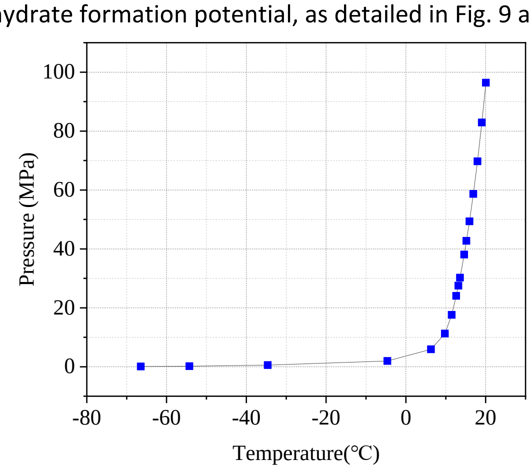

Fig. 9 Hydrate curve of impurity-containing CO_2

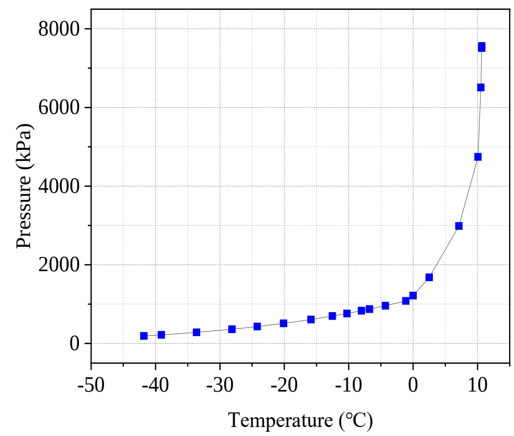

Fig. 10 Hydrate curve of pure CO_2

Based on a comparison of hydrate phase equilibrium curves, both impure CO_2 and pure CO_2 present hydrate formation risks below 10°C, but their phase behaviors exhibit key differences. The hydrate formation curve for impure CO_2 shows an acutely steepened slope in the low-temperature region (<5°C). For instance, at 5°C, the formation pressure increases by approximately 2.8 MPa compared to the pure CO_2 system (5.0 MPa vs. 2.2 MPa). Pure CO_2 exhibits a sharply steepened slope after 10°C, differing by 5°C from impure CO_2. This indicates that impurity components inhibit hydrate lattice stability through competitive adsorption, requiring higher pressure to drive nucleation. The underlying mechanism involves the coupled effects of phase transition, intensified molecular thermal motion, and precritical effects[37,38].

The critical temperature for pure CO_2 hydrate formation is 10°C (corresponding to P=2.2 MPa), whereas for impure CO_2, it decreases to 8°C (corresponding to P=3.5 MPa). This reduction is attributed to strong polar components like H_2S forming hydrogen-bonding networks with water molecules, which weakens the selective cage occupancy capability of CO_2 molecules within the hydrate lattice[39-41].

2.3 Energy Consumption Optimization Analysis for Impure CO_2 Reinjection

Calculations using OLGA software determined the pressures corresponding to fixed outlet temperatures under both high-temperature and low-temperature reinjection conditions. For high-temperature reinjection, the pressure at Aspen HYSYS stream number 18 was calculated as 14.4 MPa, whereas for low-temperature reinjection, it was 14.2 MPa.

Employing the HYSYS built-in optimizer for energy consumption optimization of the four-stage compression process, while controlling the optimal compression ratio for each stage, yielded the temperature, pressure for each compression stage, and the total energy consumption for the entire process, as detailed in Table 5 and Table 6.

Table 5 Compression Parameters and Energy Consumption for High-Temperature/Low-Temperature Reinjection of Impure CO_2

High Temperature Reinjection				Low Temperature Reinjection			
HYSYS Logistics No.	Pressure (MPa)	Temperature (℃)	Pressure ratio	HYSYS Logistics No.	Pressure (MPa)	Temperature (℃)	Pressure ratio
10	0.12	25		10	0.12	25	
11	0.48	183.5	4	11	0.48	183.5	4
12	0.48	35		12	0.48	35	
13	1.728	184.2	3.6	13	1.728	184.2	3.6
14	1.728	35		14	1.728	35	
15	5.184	161.3	3	15	5.184	161.3	3
16	5.184	35		16	5.184	35	
17	14.4	150.9	2.78	17	14.2	149.1	2.74
18	14.4	50		18	14.2	20	
Boosting energy consumption		16357.96kW		Boosting energy consumption		16305.2kW	
Cooling energy consumption		17.62kW		Cooling energy consumption		5391.38kW	
Total energy consumption		16375.58kW		Total energy consumption		21696.58kW	

Table 6 Comparison of energy consumption for pressurization of CO_2 with impurities in high/low temperature reinjection

Reinjection method	Initial temperature	Initial pressure	Reinjection temperature	Reinjection pressure	Energy consumption
High Temperature Reinjection	50℃	14.4MPa	36.05℃	15MPa	16375.58kW
Low Temperature Reinjection	20℃	14.2MPa	28.3℃	15MPa	21696.58kW

Based on Tables 5 and 6, both high-temperature (50°C) and low-temperature (20°C) reinjection utilize four-stage compression, but exhibit differences in compression ratio distribution and terminal state. The total energy consumption (compression and cooling) for high-temperature reinjection is lower than that for low-temperature reinjection.

High-temperature reinjection: Total pressure ratio increases from 0.12 MPa to 14.4 MPa. The stage compression ratios are 4 → 3.6 → 3 → 2.78, with a final stage outlet temperature of 50℃.

Low-temperature reinjection: Total pressure ratio increases from 0.12 MPa to 14.2 MPa. The stage compression ratios are 4→3.6→3→2.74, with a final stage outlet temperature of 20℃.

The key differences lie in:

1) Non-isentropic compression ratio gradient: Although the final stage compression ratio is slightly higher for high-temperature reinjection (2.78 vs. 2.74), the superior compressibility of the higher-temperature gas results in only a 52.76 kW difference in actual compression power (16357.96 kW vs. 16305.2 kW).

2) Significant disparity in cooling load: High-temperature reinjection requires only air cooling for inter-stage cooling (target temperature 35°C), consuming 17.62 kW cooling energy. Low-temperature reinjection requires refrigeration to maintain 20°C, consuming 5391.38 kW cooling energy, accounting for 24.8% of the total energy consumption.

For both high-temperature and low-temperature reinjection of impure CO_2, transportation and reinjection occur in the gaseous phase. The required compression pressure (and hence energy consumption) differs little between the different reinjection temperatures. Crucially, if the cooling temperature requirement is higher, air cooling suffices, eliminating the need for refrigeration.

Based on the above energy consumption analysis, two engineering recommendations for optimizing the energy consumption of impure CO_2 reinjection systems are proposed:

1) Thermal Management System Upgrade: Implement waste heat boilers and adsorption refrigeration modules to achieve cascaded energy utilization.

2) Intelligent Control Platform: Embed machine learning algorithms to enable real-time optimization of compression ratios and cooling temperature setpoints, responding to ambient temperature fluctuations.

The synergistic optimization through waste heat recovery and intelligent control reduces the total energy consumption of the impure CO_2 reinjection system, providing a critical technical pathway for enhancing the economic viability of carbon capture projects.

3. CONCLUSIONS

This study systematically elucidates the phase evolution patterns, flow risk characteristics, and energy optimization pathways for impurity-containing CO_2

reinjection through multiscale modeling and engineering case analyses. Key conclusions are summarized as follows:

(1) Phase Behavior and Model Selection

The Peng-Robinson (PR) equation of state achieves the lowest prediction error (average 1.89%) for phase equilibrium of impurity-containing CO_2, outperforming the SRK (3.57%) and BWRS (2.41%) models. Impurities induce critical point shifts by altering intermolecular interactions: 50% N_2 elevates critical pressure by a factor of 2.638 (7.37 MPa → 19.94 MPa) and reduces critical temperature by 66.21°C (30.95°C → –35.26°C), necessitating gaseous phase transportation to avoid multiphase flow risks. H_2 exerts the most pronounced impact on phase envelopes, with 3% H_2 expanding the bubble point curve by 18%. In contrast, H_2O and H_2S exhibit negligible critical point influence due to polarity-driven immiscibility with CO_2.

(2) Flow Assurance and Risk Boundaries

Impurity-containing CO_2 exhibits a 2.66°C lower Joule-Thomson cooling drop than pure CO_2 (104.97°C vs. 107.63°C). Light impurities (e.g., H_2) suppress overall temperature reduction via negative J-T coefficients, yet discharge temperatures consistently remain below –40°C. OLGA simulations confirm that hydrate critical formation temperature decreases from 10°C (pure CO_2) to 8°C for impurity-laden systems, with generation pressure rising by 2.8 MPa (5.0 MPa vs. 2.2 MPa) below 5°C. Dual mitigation strategies—thermal insulation optimization and thermodynamic inhibitor (THI) injection—are essential to prevent blockage risks.

(3) Energy Efficiency and Engineering Application

For the Snohvit case study's four-stage compression scheme, high-temperature reinjection (50°C) reduces total energy consumption to 16.38 MW, achieving 24.8% savings compared to low-temperature injection (20°C). This efficiency gain primarily stems from replacing refrigeration with air cooling, slashing interstage cooling load (17.62 kW vs. 5391.38 kW). Further optimization can integrate waste heat boilers with adsorption refrigeration modules for cascade utilization. Coupled with intelligent control platforms dynamically adjusting compression ratios and cooling temperatures in response to environmental fluctuations, annual energy consumption can be further reduced.

Future research should validate dynamic impurity-phase-flow coupling mechanisms via high-pressure loop experiments and investigate long-term impurity effects on mineral dissolution and storage integrity. Additionally, lifecycle pipeline optimization models leveraging digital twin technology represent a critical pathway for scaling CCUS deployment.

DECLARATION OF INTEREST STATEMENT

The authors declare that they have no known competing financial interests or personal relationships that could have appeared to influence the work reported in this paper. All authors read and approved the final manuscript.

REFERENCE

[1] Rodrigues C, Pinheiro H, De Sousa M L. Clean Energy Transition Challenge: The Contributions of Geology[J]. Affordable and Clean Energy, 2022: 47.

[2] Boot-Handford M E, Abanades J C, Anthony E J, et al. Carbon capture and storage update[J]. Energy Environ Sci, 2014, 7(1): 130-189.

[3] Leung D Y C, Caramanna G, Maroto-Valer M M. An overview of current status of carbon dioxide capture and storage technologies[J]. Renewable and Sustainable Energy Reviews, 2014, 39: 426-443.

[4] Kohl A L, Nielsen R. Gas purification [M]. Elsevier, 1997.

[5] Wetenhall B, Aghajani H, Chalmers H, et al. Impact of CO2 impurity on CO2 compression, liquefaction and transportation[J]. Energy Procedia, 2014, 63: 2764-2778.

[6] Behvandi R, Mirzaie M. A novel correlation for modeling interfacial tension in binary mixtures of CH_4, CO_2, and N_2+ normal alkanes systems: Application to gas injection EOR process[J]. Fuel, 2022, 325: 124622.

[7] Span R, Wagner W. A New Equation of State for Carbon Dioxide Covering the Fluid Region from the Triple‐Point Temperature to 1100 K at Pressures up to 800 MPa[J]. Journal of Physical & Chemical Reference Data, 1996, 25(6): 1509-1596.

[8] Aursand P, Hammer M, Munkejord S T, et al. Pipeline transport of CO2 mixtures: Models for transient simulation[J]. International Journal of Greenhouse Gas Control, 2013, 15: 174-185.

[9] Kunz O, Wagner W. The GERG-2008 Wide-Range Equation of State for Natural Gases and Other Mixtures: An Expansion of GERG-2004[J]. Journal of Chemical & Engineering Data, 2012, 57(11): 3032-3091.

[10] Albright L. Albright's chemical engineering handbook [M]. CRC Press, 2008.

[11] Banks H J, Annis P C. Comparative advantages of high CO_2 and low O_2 types of controlled atmospheres for grain storage[J]. Food Preservation by Modified Atmospheres (ed Calderon, M, and Barkai-Golan, R) Boca Raton, FL, 1990: 93-122.

[12] Moon S J, Yu S, Oh N Y, et al. Experimental and simulation study of single-matrix, all-polymeric thin-film composite membranes for CO2 capture: Block vs random copolymers[J]. Journal of Membrane Science, 2025, 715: 123496.

[13] Yu Y, Yang G, Cheng F, et al. Effects of impurities N2 and O2 on CO2 storage efficiency and costs in deep saline aquifers[J]. Journal of Hydrology, 2021, 597.

[14] Diamantonis N I, Boulougouris G C, Tsangaris D M, et al. Thermodynamic and transport property models for carbon capture and sequestration (CCS) processes with emphasis on CO2 transport[J]. Chemical Engineering Research and Design, 2013, 91(10): 1793-1806.

[15] de Koeijer G, Henrik Borch J, Drescher M, et al. CO2 transport–Depressurization, heat transfer and impurities[J]. Energy Procedia, 2011, 4: 3008-3015.

[16] Mohitpour M, Golshan H, Murray M A, et al. Pipeline design & construction: a practical approach [M]. ASME press New York, 2007.

[17] Chapoy A, Nazeri M, Kapateh M, et al. Effect of impurities on thermophysical properties and phase behaviour of a CO2-rich system in CCS[J]. International Journal of Greenhouse Gas Control, 2013, 19: 92-100.

[18] Torp T A, Gale J. Demonstrating storage of CO2 in geological reservoirs: The Sleipner and SACS projects[J]. Energy, 2004, 29(9-10): 1361-1369.

[19] You J, Wang Y, Zhou R, et al. A High-Sensitivity Three-Component Accelerometer for the Seismic Monitoring of CO2 Geological Sequestration[J]. Sensors Journal, IEEE, 2025, 25(3): 4324-4332.

[20] Peletiri S P, Rahmanian N, Mujtaba I M. CO2 Pipeline design: A review[J]. Energies, 2018, 11(9): 2184.

[21] Madani Sani F, Huizinga S, Esaklul K A, et al. Review of the API RP 14E erosional velocity equation: Origin, applications, misuses, limitations and alternatives[J]. Wear, 2019, 426-427: 620-636.

[22] McCoy S, Rubin E. An engineering-economic model of pipeline transport of CO2 with application to carbon capture and storage[J]. International Journal of Greenhouse Gas Control, 2008, 2(2): 219-229.

[23] Bai F, Lu Y. Effects of impurities on anthropogenic CO2 pipeline transport[J]. Energy & Fuels, 2024, 38(11): 9958-9966.

[24] Thu E S. Modeling of transient CO2 flow in pipelines and wells[D]: Institutt for energi-og prosessteknikk, 2013.

[25] Ge W, Chen F, Gao J, et al. Analytical multi-scale method for multi-phase complex systems in process engineering—Bridging reductionism and holism[J]. Chemical Engineering Science, 2007, 62(13): 3346-3377.

[26] Lu W, Hu H, Qi G. Effect of pipe diameter and inlet parameters on liquid CO2 flow in transportation by pipeline with large height difference[J]. Processes, 2019, 7(10): 756.

[27] Teh C, Barifcani A, Pack D, et al. The importance of ground temperature to a liquid carbon dioxide pipeline[J]. International Journal of Greenhouse Gas Control, 2015, 39: 463-469.

[28] Ebrahimi-Mamaghani A, Sotudeh-Gharebagh R, Zarghami R, et al. Dynamics of two-phase flow in vertical pipes[J]. Journal of Fluids and Structures, 2019, 87: 150-173.

[29] Ren F, Ma G, Wang Y, et al. Two-phase flow pipe network method for simulation of CO2 sequestration in fractured saline aquifers[J]. International Journal of Rock Mechanics and Mining Sciences, 2017, 98: 39-53.

[30] Zhang Z X, Wang G X, Massarotto P, et al. Optimization of pipeline transport for CO2 sequestration[J]. Energy Conversion and Management, 2006, 47(6): 702-715.

[31] Modisette J L. Equation of state tutorial; proceedings of the PSIG Annual Meeting, F, 2000 [C]. PSIG.

[32] Knoope M M J, Ramírez A, Faaij A P C. A state-of-the-art review of techno-economic models predicting the costs of CO2 pipeline transport[J]. International Journal of Greenhouse Gas Control, 2013, 16: 241-270.

[33] Svensson R, Odenberger M, Johnsson F, et al. Transportation systems for CO2––application to carbon capture and storage[J]. Energy Conversion and Management, 2004, 45(15-16): 2343-2353.

[34] Koornneef J, Spruijt M, Molag M, et al. Quantitative risk assessment of CO2 transport by pipelines--a review of uncertainties and their impacts[J]. J Hazard Mater, 2010, 177(1-3): 12-27.

[35] Holloway S, Pearce J, Hards V, et al. Natural emissions of CO2 from the geosphere and their bearing on the geological storage of carbon dioxide[J]. Energy, 2007, 32(7): 1194-1201.

[36] Akhmetova A. Thermodynamics and fluid flow models for CO2 flow assurance[D]: University of South-Eastern Norway, 2023.

[37] Turan G, Zapantis A, Kearns D, et al. Global status of CCS 2021[J]. CCS Accelerating to net zero, 2021.

[38] Umantsev A. Thermal effects of phase transformations: A review[J]. Physica D: Nonlinear Phenomena, 2007, 235(1-2): 1-14.

[39] Both A K, Gao Y, Zeng X C, et al. Gas hydrates in confined space of nanoporous materials: new frontier in gas storage technology[J]. Nanoscale, 2021, 13(16): 7447-7470.

[40] Wang X, Zhang Y, Wang F, et al. Unlocking the potential of hydrate-based carbon capture: A review of passive techniques for CO2 hydrate formation promotion[J]. Gas Science and Engineering, 2024: 205323.
[41] Zhang X, Yang H, Huang T, et al. Research progress of molecular dynamics simulation on the formation-decomposition mechanism and stability of CO2 hydrate in porous media: A review[J]. Renewable and Sustainable Energy Reviews, 2022, 167: 112820.